

Poincaré modes of light

Enrique J. Galvez and Shreeya Khadka

Department of Physics and Astronomy, Colgate University, 13 Oak Drive, Hamilton, New York
13346, U.S.A.

ABSTRACT

This article presents a study of Poincaré-mode patterns produced by superpositions of high-order Laguerre-Gauss modes in orthogonal polarization eigenstates. We cover the cases of three polarization bases: circular, linear and elliptical. We show that a variety of patterns can be created, many containing polarization singularities and multiple mappings of the Poincaré sphere onto the beam mode.

Keywords: Poincare beams, Vector beams, Laguerre-Gauss modes, Polarization

1. INTRODUCTION

Poincaré beams are a general form of vector beams. Their transverse profile carries a state of polarization that varies from point to point. These polarization-state patterns constitute partial, full or multiple mappings of the Poincaré sphere onto the transverse plane of the mode.

A general state of polarization can be constructed by a superposition of orthogonally polarized fields with distinct amplitudes and phases. Spatial modes have, in general, transverse properties in which the amplitude and phase varies across the mode. Thus, if we superimpose distinct spatial modes in orthogonal polarizations we will have modes whose a polarization state varies with the transverse coordinates.

Early work with these types of modes focused primarily on cases that involved first-order modes.¹ This work gave rise to the study of vector beams. These are beams with a transverse profile that consists of states of linear polarization with varying orientations across the profile. Modes in which the polarization is parallel to the radius vector from the center of the beam are called radial vector beams, and those with polarization tangential to the center of the beam are called azimuthal vector beams. These beams have found application in charged-particle acceleration² and manipulation.³ One way to produce these modes is to combine first-order Laguerre-Gauss modes of opposite helicity and circular polarization eigenstates. Because the spatial modes have the same order, their amplitudes are the same but their phases vary with the transverse angular coordinate in opposite ways, resulting in linearly polarized states of different orientations. Other equivalent approaches involve superimposing Hermite-Gauss modes with opposite linear polarization.⁴

The first-order Laguerre-Gauss modes in orthogonal linear polarization eigenstates give rise to modes that contain elliptical polarization states in their transverse profile.⁷ However, the use of spatial modes of different order results in a much richer variety of polarization patterns,⁵ giving rise to Poincaré modes,⁶ which are modes that carry all the states of the Poincaré sphere. The systematic study of the latter modes is the subject of our report.

In this article we investigate the vector patterns that can be generated with Laguerre-Gauss modes in any pair of polarization eigenstates. In Section 2 we define the theoretical formalism. Section 3 describes the apparatus that we used, and Section 4 presents our results in three subsections, one for each polarization basis: circular, linear and elliptical. Section 5 presents discussions and conclusions.

Further author information: (Send correspondence to E.J.G.)
E.J.G.: E-mail: egalvez@colgate.edu, Telephone: 1 315 228 7205
Proceedings of SPIE **8274**, 827433 (2012).

2. THEORETICAL FORMALISM

This work involves the superposition of two Laguerre-Gauss modes, each in orthogonal polarization states. The amplitude of a Laguerre-Gauss mode is defined in cylindrical coordinates (r, ϕ, z) as⁹

$$LG_p^\ell = A_{p,\ell} r^{|\ell|} e^{i\ell\phi} GL_p^{|\ell|}, \quad (1)$$

where

$$A_{p,\ell} = \left(\frac{p! 2^{|\ell|+1}}{\pi(|\ell| + p)!} \right)^{1/2} \frac{1}{w^{|\ell|+1}} \quad (2)$$

is a normalization constant;

$$G = e^{-r^2/w^2} \quad (3)$$

is the gaussian envelope, with w being the beam width (or spot); and $L_p^{|\ell|}$ is the associated Laguerre function of $2r^2/w^2$. For simplicity we neglect other usual terms in this type of mode, such as the radius of curvature of the wavefront and the Gouy phase. These terms are relevant when discussing propagation effects, which is not the focus of this work. The index p corresponds to the number of radial nodes of the mode. The mode has the well known azimuthal phase term, $\exp(i\ell\phi)$, where ℓ is an integer that specifies the winding of the phase around the beam in multiples of 2π . The index ℓ is also known as the topological charge. We note that the choice of positive sign in the exponent responds to choosing a wave propagator of the form $\exp i(kz - \omega t)$, where k and ω are the wavenumber and the angular frequency of the wave.

We choose an unconventional but convenient method to define the state of polarization:^{4,8}

$$\hat{e}_{\theta,\chi} = \hat{e}_R e^{+i\theta} \cos \chi + \hat{e}_L e^{-i\theta} \sin \chi, \quad (4)$$

where \hat{e}_R and \hat{e}_L represent the states of circular polarization, right and left, respectively, defined as

$$\hat{e}_R = \frac{1}{\sqrt{2}}(\hat{e}_X - i\hat{e}_Y) \quad (5)$$

and

$$\hat{e}_L = \frac{1}{\sqrt{2}}(\hat{e}_X + i\hat{e}_Y), \quad (6)$$

with \hat{e}_X and \hat{e}_Y denoting the states of linear polarization along the transverse X and Y directions. The choice of signs defining the circular polarization states in terms of the linear polarization eigenstates also correlate with the choice of propagator phase.¹⁰

The circular polarization states are most convenient for defining the state of polarization. This is because the angles χ and θ independently determine the ellipticity and orientation of the state of polarization, as shown in Fig. 1. The angle χ varies between 0 and $\pi/2$, and corresponds to half the polar angle on the Poincaré sphere, as shown in Fig. 1(b). The ellipticity of the state is defined by

$$\epsilon = \frac{b}{a} = \tan(\pi/4 - \chi), \quad (7)$$

where a and b are the semimajor and semiminor axes of the ellipse, respectively. The orientation of the ellipse θ , is the angle that the semimajor axis of the ellipse forms with the x -axis. It is also half the longitude on the Poincaré sphere, as shown in Fig. 1(b). As is well known, the north and south poles of the sphere correspond to the right and left circularly polarized states, respectively, with the equator corresponding to the states of linear polarization with different orientations.

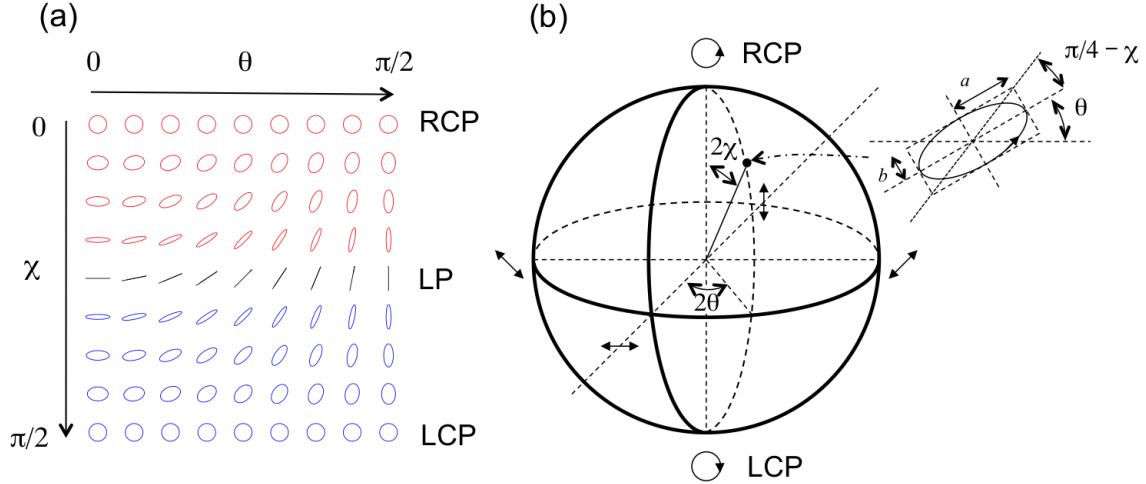


Figure 1. (a) States of polarization as a function of the angles χ and θ , defined in Eq. 4. Red and blue colors represent right-handed and left-handed polarization states, respectively, whereas black represents linear polarization. (b) Poincaré sphere showing all the states of polarization represented on the surface of a sphere.

3. APPARATUS

We prepared the Poincaré modes using a polarization interferometer, shown in Fig. 2. A circularly-polarized laser beam from a helium-neon laser is passed through a polarizer with transmission axis at 45 degrees to the horizontal. A polarizing beam splitter splits the beam. The thru beam with linear polarization along the x (horizontal) direction goes through a binary forked grating, which encodes the Laguerre-Gauss mode $LG_{p_1}^{\ell_1}$ in first order diffraction. The other arm of the interferometer channels the light with polarization aligned with the y (vertical) direction. In this arm the light is incident onto another binary forked grating that encodes the mode $LG_{p_2}^{\ell_2}$ in first order.

A quarter-wave plate with fast axis forming an angle φ with the horizontal was placed after the interferometer. It changed the polarization of the component beams into a state with ellipticity defined by $\chi = \varphi$, and orientation $\theta = \varphi/2$. This prepared the polarization eigenstates of each of the spatial modes. This way, when $\varphi = 0$ the polarization eigenstates were \hat{e}_X and \hat{e}_Y , and when $\varphi = \pi/4$, they were \hat{e}_R and \hat{e}_L . Thus by just varying φ we could obtain all the ellipticities. If we were to add half-wave plate after the quarter-wave plate (which we did not do) we could in principle access all elliptical orientations. By tilting a thin glass blank placed in one of the arms we inserted a relative phase 2α between the two modes.

In the experiments reported here we prepared modes with $p_1 = 0$ and $\ell_1 = 2$, and $p_2 = 0$ and $\ell_2 = 0$. Other combinations are reported elsewhere.⁸ The intensity of the resulting mode, with no polarization filtering, had the smooth appearance shown in Fig. 2. As described next, the bland appearance is misleading because the it hid rich polarization patterns encoded in the transverse coordinates.

We diagnosed these polarization patterns by blocking individual states of polarization with an otherwise standard polarimetry technique. For sake of clarity, we explain this in detail. If we wanted to block the elliptically polarized state specified by χ and θ , we first passed the light through a half-wave plate oriented an angle $\theta/2$. This rotated the semimajor axis of the ellipse to become horizontal. It also changed the handedness of the ellipse. A quarter-wave plate with fast axis either horizontal or vertical changed the state from being elliptical to linear oriented at $\pi/4 - \chi$ with the horizontal. The choice of vertical or horizontal depended on the handedness of the state before the quarter-wave plate. A subsequent half-wave plate with fast axis forming an angle $\pi/8 - \chi/2$ with the horizontal flipped the orientation to be along the horizontal. A polarizer with transmission axis vertical blocked the light. With these settings, other polarization states were transmitted with various amplitudes. The resulting beam was imaged by a digital camera. The advantage of this particular method is that the half-wave plates control θ and χ independently. As will be shown later, for the modes that we considered, two points in

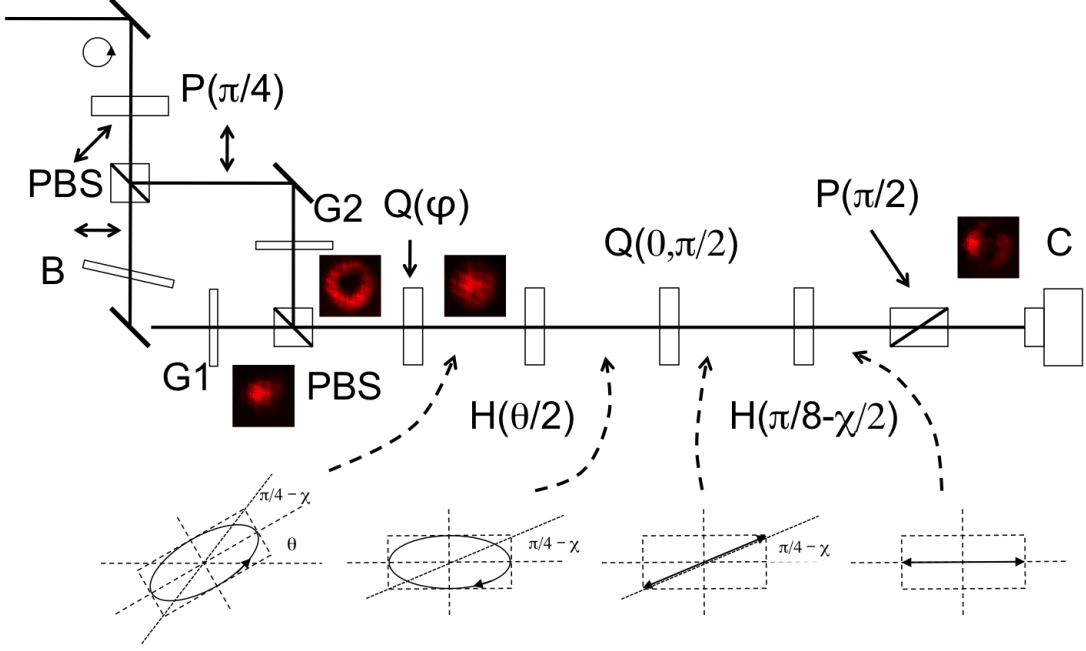


Figure 2. Schematic of the apparatus used to prepare and diagnose the Poincaré modes. It uses polarizing beam splitters (PBS), forked gratings (G1 and G2), glass blank (B) polarizers (P), half-wave plates (H), quarter-wave plates (Q) and a digital camera (C). Inserted images correspond to the case where $p_1 = 0$, $\ell_1 = 2$, $p_2 = 0$ and $\ell_2 = 0$. The detection scheme consisting of three waveplates blocked any state of polarization by transforming it into horizontally polarized before going through a vertical polarizer.

the transverse mode of the beam, opposite across the center of the beam, had the same polarization state. Thus, passage of the beam through our detection apparatus revealed a mode with two intensity minima, as shown in Fig. 2.

4. RESULTS

We define the general Poincaré mode by

$$V_{p_1, \ell_1, p_2, \ell_2} = \frac{1}{\sqrt{2}} (LG_{p_1}^{\ell_1} e^{i\alpha} \hat{e}_{\theta, \chi} + LG_{p_2}^{\ell_2} e^{-i\alpha} \hat{e}_{\theta + \pi/2, \pi/2 - \chi}) \quad (8)$$

The two polarization eigenstates are antipodes on the Poincaré sphere. We will divide our presentation into three cases, with each case specifying the use of a particular polarization basis associated to the component spatial modes. We will also limit ourselves to the cases with $p_1 = p_2 = 0$ for simplicity.

4.1. Circular Basis

The Poincaré mode for this case is given by

$$V_{0, \ell_1, 0, \ell_2} = G \left(A_{0, \ell_1} r^{|\ell_1|} e^{i(\ell_1 \phi + \alpha)} \hat{e}_R + A_{0, \ell_2} r^{|\ell_2|} e^{i(\ell_2 \phi - \alpha)} \hat{e}_L \right). \quad (9)$$

This equation can be written in the following form:

$$V_{0, \ell_1, 0, \ell_2} = NG e^{i(\ell_1 + \ell_2)\phi/2} (\cos \chi e^{i\theta} \hat{e}_R + \sin \chi e^{-i\theta} \hat{e}_L), \quad (10)$$

where

$$\chi = \tan^{-1} \frac{A_{0, \ell_2} r^{|\ell_2|}}{A_{0, \ell_1} r^{|\ell_1|}}, \quad (11)$$

$$\theta = (\ell_1 - \ell_2)\phi/2 + \alpha, \quad (12)$$

and N is a normalization constant.

Figure 3(a) shows the polarization map corresponding to $\ell_1 = 2$ and $\ell_2 = 0$. We can observe that the beam profile contains in principle all the states of polarization repeated in two angular sectors. Equations 11 and 12 reveal that this case provides a simple mapping of states on the Poincaré sphere to points on the transverse mode: The ellipticity depends exclusively on r and the orientation depends exclusively on ϕ . The central spot is the left circular polarized state, corresponding to the south pole on the sphere. As r increases the ellipticity decreases, reaching linear polarization at

$$r_v = \left(\frac{A_{0,\ell_2}}{A_{0,\ell_1}} \right)^{1/(|\ell_1| - |\ell_2|)}. \quad (13)$$

As r continues to increase, the handedness of the ellipse reverses and the ellipticity increases, reaching right circular polarization at $r = \infty$. Following a path with fixed azimuthal angle ϕ from $r = 0$ is equivalent to following a meridian on the sphere that starts at the south pole and ends at the north pole. The states of same r but varying ϕ have the same ellipticity but different orientation, with equivalent points on the Poincaré sphere belonging to the same parallel on the sphere (i.e., having the same latitude), as shown in Fig 3(b). Figure 3(c)

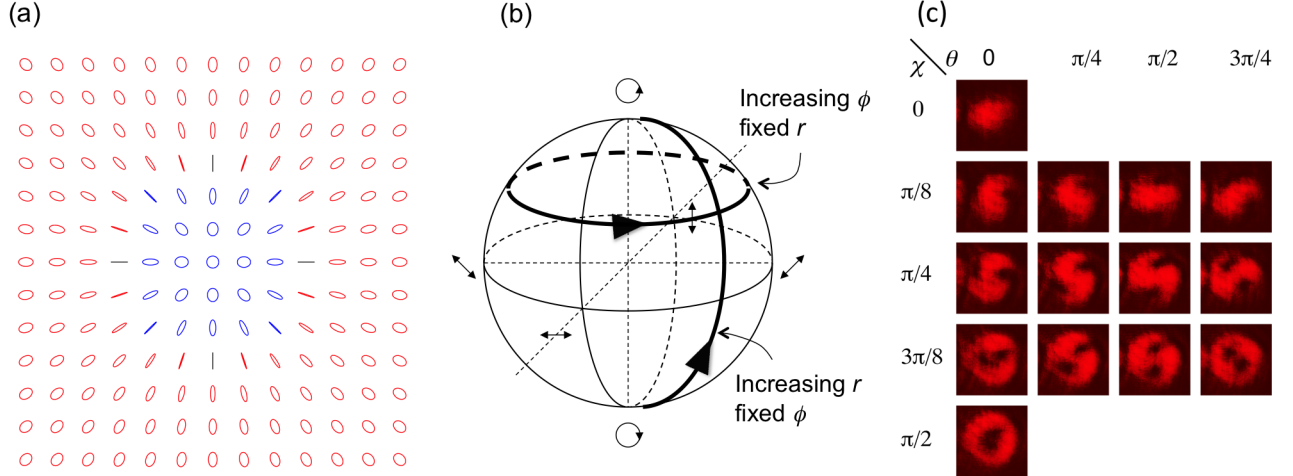


Figure 3. (a) Polarization-state map obtained by combining $\ell_1 = 2$ and $\ell_2 = 0$ spatial modes in the circular polarization basis. (b) Paths on the Poincaré sphere followed by the state of polarization for points of increasing transverse angle ϕ and fixed radius r , and points of increasing radius r and fixed transverse angle ϕ . (c) Images of the mode after blocking specific polarization states.

shows the data obtained by blocking states with selected values of χ and θ . The data is consistent with the map of Fig. 3(a). The figure shows that the distance between each minima and the center of the beam decreases with increasing χ , consistent with the nulled state of polarization following trajectories along meridians on the Poincaré sphere such as the one shown in Fig 3(b). The case $\chi = \pi/2$ corresponds to nulling the left circular polarization state, located at the center of the beam. When $\chi = \pi/4$, corresponding to nulling the state of linear polarization, shows two minima in the image. As the orientation of the nulled state is changed via θ we see that the minima rotate about the center of the beam, consistent with the expectations. This is more clearly seen for $\chi = 3\pi/8$, where the minima are located closer to the center.

The center of the beam of Fig. 3(a) is a “C-point” polarization singularity—a location where the orientation of the ellipse is undefined.^{11,12} The mode shows linear polarization states distributed along a circle of radius $r = r_v$. This “L-line” separates mappings of states with different handedness. It is a singularity where the handedness of the ellipse is undefined.¹³ For the case when $\ell_1 = -\ell_2$ the entire mode is composed of linearly

polarized states with orientations depending on the angular coordinate,⁸ and with the center being a Poincaré-Hopf vector singularity.¹⁴ The latter is a case where one Stokes parameter $S_3 = 0$, and the other two, S_1 and S_2 are undefined.⁸

4.2. Linear Basis

Poincaré modes in the linear polarization basis are quite different from the previous case. The expression for the modes is:

$$V_{0,\ell_1,0,\ell_2} = Ge^{i(\ell_1+\ell_2)\phi/2} \left(A_{0,\ell_1} r^{|\ell_1|} e^{i(\ell_1-\ell_2)\phi/2+\alpha} \hat{e}_X + A_{0,\ell_2} r^{|\ell_2|} e^{-i(\ell_1-\ell_2)\phi/2+\alpha} \hat{e}_Y \right). \quad (14)$$

We can rewrite this equation so that it has the same form as Eq. 10:

$$V_{0,\ell_1,0,\ell_2} = NG e^{i(\ell_1+\ell_2)\phi/2} (\cos \chi' e^{-i\theta'} \hat{e}_X + \sin \chi' e^{i\theta'} \hat{e}_Y). \quad (15)$$

The primed angles are the same as before $\chi' = \chi$ and $\theta' = \theta$, defined by Eqs. 11 and 12, respectively. However, they no longer specify the ellipticity and orientation of the polarization state.

Figure 4(a) shows the polarization map for the linear case, using the same spatial modes as before. The map is quite different from the map for circular polarization. However, we can easily understand it. Since Eq. 15 has the same form as Eq. 10, it can be shown that radial trajectories from the center of the mode correspond to geodesics that connect the two basis states, and circular trajectories around the center of the beam correspond to the same parallel on the sphere when the poles are the eigenstates of linear polarization, as shown in Fig. 4(b).

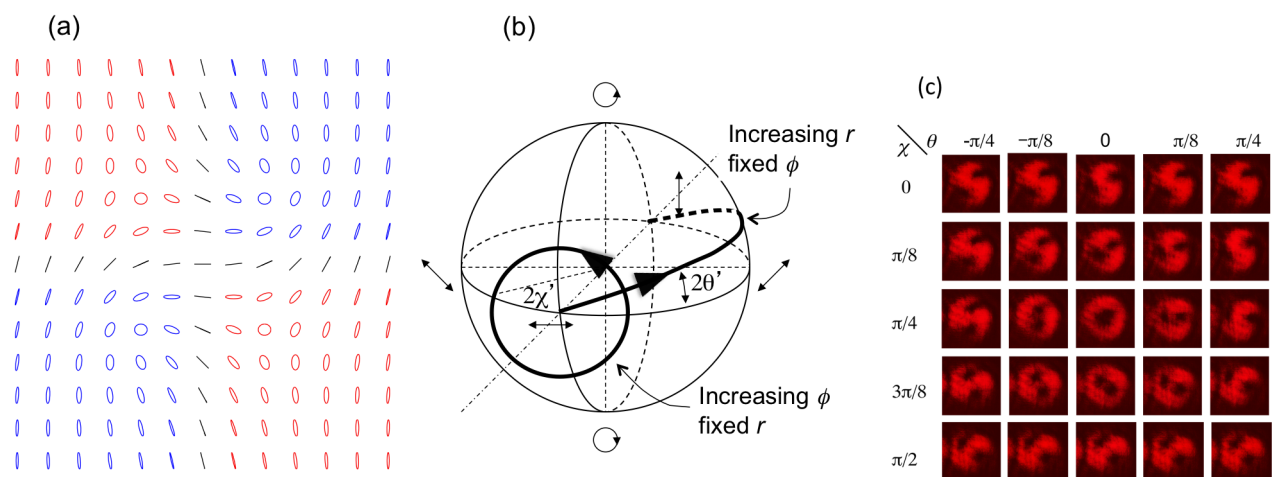


Figure 4. (a) Polarization-state map obtained by combining $\ell_1 = 2$ and $\ell_2 = 0$ spatial modes in the linear polarization basis. (b) Poincaré sphere showing the paths followed by the state of polarization for increasing transverse angle ϕ and fixed radius r , and points of increasing radius r and fixed transverse angle ϕ . (c) Images showing the mode after blocking polarization states specified by χ and θ

In Fig 4(c) we show the experimental verification of the mode, similar to the previous case. Let us consider the case when the nulled state has linear polarization ($\chi = \pi/4$). As we increase θ from 0 we see two minima move outward along the x -direction in the beam image, and when θ is decreased from 0, the minima move outward along the y -direction. This is consistent with the polarization map of Fig. 4(a). The circular polarization states ($\chi = 0, \pi/2$) are independent of θ , as shown in the top and bottom row of images in Fig. 4(c). For other polarization states such as those with $\chi = \pi/8$, the minima describe a curved trajectories as a function of θ . The trajectories go around the circular state and are bound by the linear trajectories, or L-lines.

As we change χ , the location of the nulled state follows the great semicircle that connects one linear polarization eigenstate to the other. On the beam profile, the minima go from one location to another one following a curved trajectory, as shown in the Fig. 4(c).

The mode of Fig.4 shows four Poincaré-sphere poles distributed in a quadrupole configuration. An interesting variation of this case, shown elsewhere,⁸ is when $\ell_1 = -\ell_2$. In this case all points with the same value of ϕ are in the same polarization state. These states correspond to the equator of the sphere that has the linear eigenstates (\hat{e}_X, \hat{e}_Y) as the poles. The central point is a polarization singularity that has all ellipticities, points where the Stokes parameter $S_1 = 0$, and the other two, S_2 and S_3 , are undefined.

4.3. Elliptical Basis

We now present a case that to our knowledge has not been investigated before: a Poincaré mode with elliptical polarization eigenstates. As mentioned earlier, our apparatus used a quarter-wave plate rotated by an angle φ to produce a state defined by $\chi = \varphi$ and $\theta = \varphi/2$. Setting $\varphi \neq 0, \pi/4$ results in elliptical polarization eigenstate, giving rise to skewed polarization patterns. Figure 5(a) shows the case when $\varphi = \pi/8$.

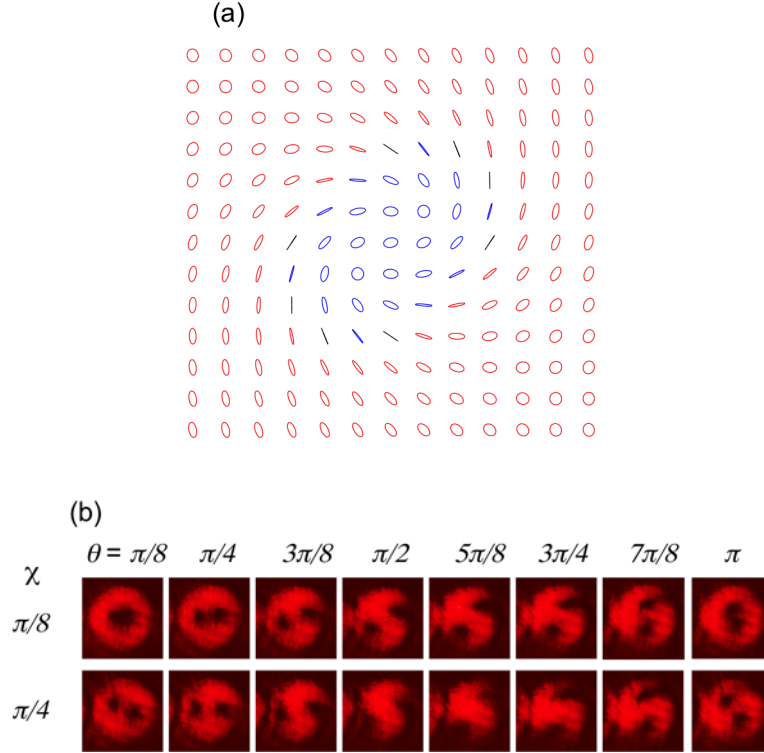


Figure 5. (a) Polarization-state map obtained by combining $\ell_1 = 2$ and $\ell_2 = 0$ spatial modes in the polarization basis with elliptical eigenstates with $\chi = \pi/8$ and $\chi = \pi/4$, and its orthogonal counterpart.(b) Images of the mode after blocking specific polarization states.

In the case of circular eigenstates, the central minimum, corresponding to a circularly polarized state, remains stationary independently of θ . In the case of linearly polarized eigenstates, the central minimum splits into two as θ is changed from zero, and the two minima move along straight vertical or horizontal trajectories, depending on the value of θ . This has been discussed before, in connection with Figs. 3 and 4. The case of elliptically polarized eigenstates is intermediate between the other two. As we vary θ from zero, two minima appear, and subsequently describe closed loops. For elliptical states with $0 < \chi < \pi/8$ two minima describe closed loops, so that for every π -change in θ each spot describes a loop. For $\chi > \pi/8$ the two minima describe one larger loop around the entire beam for a 2π -change in θ , as seen in Fig. 5.

5. DISCUSSION

In summary, we present a study of a wide range Poincaré modes formed by Laguerre-Gauss eignemodes in any pair of polarization eigenstates. We find patterns of various types that can be understood as mappings from the

Poincaré sphere to the transverse plane of the beam. We observe various types of polarization singularities.

Our study is limited to a superposition of collinear Laguerre-Gauss eigenmodes. Noncollinear superpositions and other spatial-mode bases will give rise to other interesting patterns.

Recent studies of polarization singularities have featured the study of singularities created when initially plane waves of light propagate through inhomogeneous media.^{15–19} It would be interesting to study such propagation effects when Poincaré modes are sent through inhomogeneous media.

ACKNOWLEDGMENTS

We thank W.H. Schubert and S. Nomoto for early contributions, and G. Milione and F. De Zela for stimulating discussions. This work was funded by National Science Foundation grant PHY-0903972, Air Force contract FA8750-11-2-0034, and by Colgate University.

REFERENCES

1. Q. Zhan, “Cylindrical vector beams: from mathematical concepts to applications,” *Adv. Opt. Photon.* **1**, 1–57 (2009).
2. J.R. Fontana R.H. and Pantell, “A high-energy, laser accelerator for using the inverse Cherenkov effect.” *J. Appl. Phys.* **54**, 4285–4288 (1983).
3. S. Quabis, R. Dorn, M. Eberler, O. Glöckl, and G. Leuchs, “Focusing light to a tighter spot,” *Opt. Commun.* **179**, 1–7 (2000).
4. E.J. Galvez, “Vector beams in free space,” in *The Angular Momentum of Light* D.L. Andrews and M. Babiker eds. (Cambridge, to be published, 2012).
5. C. Maurer, A. Jesacher, S. Fürhapter, S. Bernet, and M. Ritsch-Marte, “Tailoring of arbitrary optical vector beams,” *New J. Phys.* **9**, 78–1–20 (2007).
6. A.M. Beckley, T.G. Brown, and M.A. Alonso, “Full Poincaré beams,” *Opt. Express* **18**, 10777–10785 (2010).
7. G. Milione, H.I. Sztul, R.R. Alfano, and D.A. Nolan, “Stokes polarimetry of a hybrid vector beam from a spun elliptical core optical fiber,” *Proc. SPIE* **7613**, 761305-10 (2009).
8. E.J. Galvez, S. Khadka, W.H. Schubert, and S. Nomoto, “Poincaré-beam patterns produced by non-separable superpositions of Laguerre-Gauss and polarization modes of light” (to be published).
9. M.W. Beijersbergen, L. Allen, H.E.L.O. van der Veen, J.P. Woerdman, “Astigmatic laser mode converters and transfer of orbital angular momentum,” *Opt. Commun.* **96**, 123–132 (1993).
10. E. Hecht, *Optics* (Addison-Wesley, 2002).
11. J.F. Nye, *Natural Focusing and Fine Structure of Light* (IOP, 1999).
12. M.V. Berry and M.R. Dennis, “Polarization singularities in isotropic random vector waves,” *Proc. R. Soc. Lond. A* **457**, 141–155 (2001).
13. J.F. Nye, “Line singularities in wave fields,” *Proc. R. Soc. Lond. A* **387**, 105–132 (1983).
14. I. Freund “Polarization singularity indices in Gaussian laser beams,” *Opt. Commun.* **201**, 251–270 (2002).
15. M.S. Soskin, V. Denisenko, and I. Freund, “Optical polarization singularities and elliptic stationary points,” *Opt. Lett.* **28**, 1473–1477 (2003).
16. F. Flossmann, U.T. Schwarz, M. Maier, and M.R. Dennis, “Polarization singularities from unfolding an optical vortex through a birefringent crystal,” *Phys. Rev. Lett.* **95**, 253901 1-4 (2005).
17. R.I. Egorov, M.S. Soskin, D.A. Kessler, and I. Freund, “Experimental measurements of topological singularity screening in random paraxial scalar and vector optical fields,” *Phys. Rev. Lett.* **100**, 103901 1–4 (2008).
18. F. Flossmann, K. O’Holleran, M.R. Dennis, and M.J. Padgett, “Polarization singularities in 2D and 3D speckle fields,” *Phys. Rev. Lett.* **100**, 203902 1–4 (2008).
19. I.O. Buinyi, V.G. Denisenko, and M.S. Soskin, “Topological structure in polarization resolved conoscopic patterns for nematic liquid crystal cells,” *Opt. Commun.* **282**, 143–155 (2010).